aerospace

MDPI

Article

Condensed Combustion Products Characteristics of HTPB/AP/Al Propellants under Solid Rocket Motor Conditions

Xue-Li Liu, Song-Qi Hu, Lin-Lin Liu * and Yan Zhang

Science and Technology on Combustion, Internal Flow and Thermo-Structure Laboratory, Northwestern Polytechnical University, Xi'an 710072, China
* Correspondence: lll@nwpu.edu.cn; Fax: +86-029-88493406

Abstract: Condensed combustion products (CCPs) generated during the combustion of aluminized propellants can reflect invaluable information about the combustion mechanisms of propellants. CCPs of hydroxyl-terminated polybutadiene/ammonium perchlorate/aluminum (HTPB/AP/Al) propellants were collected using an experimental apparatus capable of controlling pressure fluctuations within 0.3 MPa, and their microscopic morphologies, particle size distributions, and chemical compositions were characterized using a scanning electron microscope (SEM), laser particle size analyzer, energy disperse spectroscopy (EDS), X-ray diffraction (XRD) and complexometric titration. The results showed that the size of CCPs presented a bimodal distribution, with modes at ~5 μm and ~100 μm; particles less than 2 μm were spherical, with smooth surfaces. The main components of CCPs were C, AlN, $AlCl_3$, Al_2O_3, Fe_2O_3 and Al, with Al_2O_3 being the most abundant. The combustion efficiency of aluminum increased by 3.27% when the size of virgin aluminum particles decreased from 23 μm to 13 μm, but the content of catocene (a burning-rate catalyst) and fine AP (1 μm) had little effect on combustion efficiency. Higher combustion efficiencies and smaller agglomeration sizes can be achieved at higher pressures, due to the positive correlation between pressure and the driving forces for aluminum particles exciting the burning surface.

Keywords: condensed combustion product (CCP); HTPB/AP/Al propellant; aluminum agglomeration; combustion efficiency

Citation: Liu, X.-L.; Hu, S.-Q.; Liu, L.-L.; Zhang, Y. Condensed Combustion Products Characteristics of HTPB/AP/Al Propellants under Solid Rocket Motor Conditions. *Aerospace* **2022**, *9*, 677. https://doi.org/10.3390/aerospace9110677

Academic Editor: Fabrizio Ponti

Received: 26 September 2022
Accepted: 28 October 2022
Published: 2 November 2022

1. Introduction

Composite propellants used in solid rocket motors are composed of polymeric matrix loaded with solid oxidizers, metal fuels, and some functional additives [1–3]. Of these, hydroxyl-terminated polybutadiene/ammonium perchlorate/aluminum (HTPB/AP/Al) composite propellants have been widely used in micro-thrusters, rockets launch vehicles and missile propulsion systems, because of their cheap cost, excellent combustion and mechanical characteristics [4–7]. Al plays an important role in improving energetic performance and damping combustion instabilities [8–12]. However, aluminized composite propellants exhibit complex combustion behavior due to the agglomeration of aluminum, and particles of a large size generated by the agglomeration of aluminum may produce unwanted effects such as nozzle erosion, slag accumulation and nozzle two-phase loss [13,14]. Therefore, it is necessary to fully understand the combustion mechanism of aluminized propellants.

Condensed combustion products (CCPs) are generated from the aggregation, splitting, and combustion behavior of aluminum droplets on the burning surface or gas reaction zone [15–18]. A great deal of useful information regarding the mechanisms of agglomeration and combustion may potentially be obtained from the particle size distribution, morphology, and composition of CCPs [19–22]. However, it is difficult to collect CCPs in the combustion chamber, due to the extreme conditions such as high pressure, temperature,

and gas velocity within. Therefore, CCPs are mainly studied based on the quench method, with the quench medium at the bottom of the closed combustion chamber, at present.

Jeenu et al. [23–25] measured the size distribution of condensed combustion products collected by the quench bomb. Experimental results showed that aluminum agglomerations could be divided into two different types: so-called "matrix" agglomeration whose surface is dispersed with many aluminum droplets, and sphere, with an alumina cap structure on one side, whose particle size tends to be smaller than that of the "matrix" agglomeration. In addition, two types of fine oxide particles, namely micron oxide particles with sizes ranging from 2 to 10 μm, and smoke oxide particles with sizes ranging from 1 to 2 μm, which are more prevalent in CCPs, were reported by Babuk et al. [19,26].

Anand et al. [27] investigated the influence of AP particle size on CCPs particle size, and results showed that the Al agglomerate size increased at higher coarse AP sizes ($\geq$250 μm) but decreased at finer AP sizes ($\leq$75 μm). Glotov et al. [28] indicated that the addition of RDX in propellants intensified the agglomeration of Al, due to the fact that molten aluminum would remain in the molten RDX on the burning surface. Sambamurthi [29] reported that the particle size of CCPs first increased and then decreased when the size of Al powder increased from 5 μm to 30 μm. However, nano-aluminum experienced significant agglomerations (of size <5 μm) during the process of propellant combustion, which was reported by Jayaraman et al. [30,31].

Tejasvi et al. [32] explored the effect of chamber pressure on CCPs, and the results showed that the average particle size of CCPs decreased by 36% when the operating pressure increased from 0.1 MPa to 0.9 MPa. Babuk et al. [33] indicated that the mass fraction of Al in CCPs collected at 1 MPa was 33–46%, while Al content in CCPs generated at 6 MPa was basically negligible. Yuan et al. [34] reported that the burning rate was the controlling factor in the diameter of aluminum agglomerations at different operating pressures, because the agglomeration process occurred in the reaction layer adjacent to the burning surface.

The characteristics of CCPs are highly sensitive to the collection methods [23,28,35], but collection devices in the aforementioned studies generally have a greater heat loss and difficulty in maintaining pressure, due to the small amount of propellant samples and the sealed container. To overcome these limitations, the present study develops a collection system that could collect all CCPs generated by propellant combustion under conditions similar to a real solid rocket motor combustion chamber, and the effect on the CCPs of varying the initial pressure, Al and AP particle sizes, and catalyst burning rate was investigated. Moreover, the influence of aluminum agglomeration during propellant combustion on both the particle size distribution of CCPs and the combustion efficiency of aluminum, was revealed. The results from this study are expected to shed new light on the combustion mechanisms of aluminized propellants, thereby aiding in the development of solid propellants.

2. Constant Pressure Collection System

2.1. Principle of Pressure Maintenance

A constant pressure is required during the propellant combustion process, but the nozzle cannot be used behind the combustion chamber because some of the characteristics of CCPs may be changed by sustained acceleration from the nozzle; additionally, some CCPs may be trapped in the combustion chamber. In this study, the pressure in the combustion chamber was controlled through the movement of a piston, as illustrated in Figure 1.

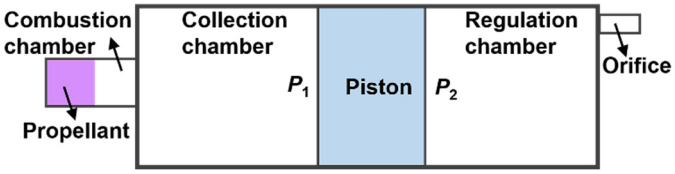

Figure 1. Schematic diagram of the pressure maintenance principle.

The combustion chamber, shown on the left-hand side in Figure 1, is where the propellant grain is burned, and the right-hand side of the combustion chamber shows the collection chamber used to cool and store CCPs, with a piston used to isolated the collection and regulation chambers. The regulation chamber provides space for the piston to move, and orifices with different effective flow areas at the outlet are used to regulate the mass flow rate of gas.

In the experiments conducted in this study, all the chambers were charged with inert gas at the same pressure, prior to providing a combustion environment for the propellant; N_2 was used as the inert gas in this paper, due to its unreactive nature. Once the propellant grain is ignited, the combustion chamber pressure rises, forcing the piston to move to the right; however, this increase in pressure can be prevented by controlling the movement of the piston relative to the mass flow rate at the orifice, thereby maintaining a constant pressure in the combustion chamber throughout the propellant combustion process.

2.2. Experimental System

A schematic of the CCPs collection system based on the pressure maintenance principle is shown in Figure 2. N_2 was used to replace the air in the combustion chamber by using a vacuum pump and a high-pressure cylinder to prevent reactions between the air and CCPs. The end-burning propellant grain with a diameter of 40 mm and a length of 30 mm, was burned in the combustion chamber, whose length is 195 mm, and the combustion products were passed into the large collection chamber with a diameter of 500 mm and an initial length of 350 mm, which varies with the movement of the piston. The discharge of gas in the regulation chamber was controlled by a solenoid valve, and the pressure in the combustion chamber, which was maintained by moving the piston, and recorded using a pressure transmitter.

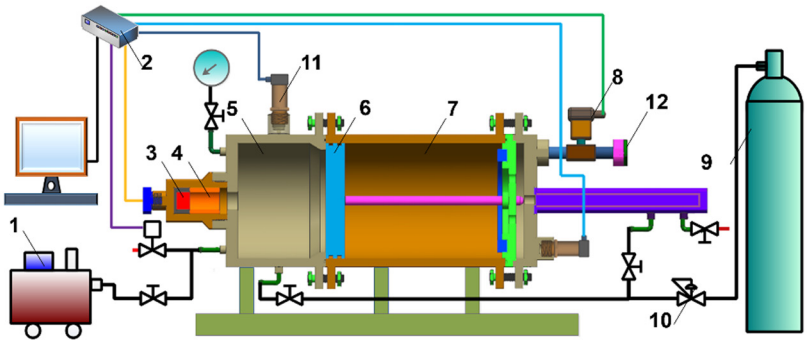

Figure 2. Schematic diagram of CCPs collection system. 1. vacuum pump 2. signal collector 3. propellant grain 4. combustion chamber 5. collection chamber 6. piston 7. regulation chamber 8. solenoid valve 9. High-pressure cylinder of N2 10. valve 11. pressure sensor 12. Exhaust outlet.

3. CCPs Collection and Analysis Experiments

3.1. Propellant Formulation

The baseline propellant formulation (labelled as 1#) used in this study consisted of HTPB binder system (13 wt%), catocene (2 wt%), AP with a particle size of 200–300 μm (45 wt%), AP with a particle size of 105–150 μm (25 wt%), and Al with a particle size of

23 μm (15 wt%). Three additional propellant formulations were also used in this study (labelled as 2#, 3#, and 4#, respectively), as listed in Table 1.

Table 1. Propellant formulations used.

Propellant No.	HTPB (wt%)	Catocene (wt%)	AP (wt%)			Al (wt%)	
			200–300 μm	105–150 μm	1 μm	23 μm	13 μm
1#	13	2	45	25	0	15	0
2#	13	2	40	25	5	15	0
3#	13	2	40	25	5	0	15
4#	15	0	40	25	5	0	15

3.2. CCPs Collection

The operating pressure has a significant influence on CCPs characteristics, and to account for pressure fluctuations during the combustion process, this pressure is normally represented using the time-averaged chamber pressure, $\overline{P}$, calculated as follows:

$$\overline{P} = \frac{\int_{t_A}^{t_B} p\mathrm{d}t}{\Delta t} \tag{1}$$

where, t_A and t_B are the start and end times of propellant combustion, respectively; Δt is burning time obtained from the experimental pressure-time curve, as shown in Figure 3.

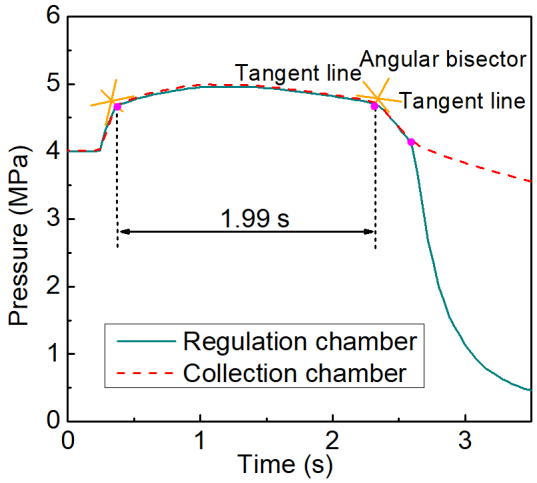

Figure 3. Experimental pressure-time curves of propellant combustion.

Figure 3 shows that combustion chamber pressure experiences a rapid increase during the ignition stage, plateaus during the combustion process, and decreases sharply after combustion. Point A and point B represent the start point and end point of the combustion process, respectively, and they are determined according to Figure 3.

Experiments were carried out at initial pressures of 4 MPa and 6 MPa, and the pressure data tested in the experiments are shown in Table 2. In addition, the maximum pressure fluctuation, ΔP, was used to represent the pressure-holding capacity of the device, as follows:

$$\Delta P = \max\left(\left|\overline{P} - P_{\max}\right|, \left|\overline{P} - P_{\min}\right|\right) \tag{2}$$

where, $P_{\max}$ and $P_{\min}$ are the maximum and minimum pressures during combustion, respectively.

Table 2. Experimental conditions and results.

Propellant No.	P_0 [a] (MPa)	L [b] (mm)	Δt (s)	$\overline{P}$ (MPa)	ΔP (MPa)
1#	4	80	0.21	4.54	0.15
1#	6	80	0.18	6.57	0.23
1#	6	120	0.23	6.66	0.21
2#	4	80	0.22	4.83	0.18
2#	6	80	0.24	7.03	0.23
3#	4	80	0.24	5.04	0.22
3#	6	80	0.16	6.90	0.24
4#	4	80	0.15	5.03	0.24
4#	6	80	0.23	6.99	0.16

a. The initial pressure, b. the length of the combustion chamber.

Table 2 indicated that chamber pressure remained almost constant during the combustion process of the propellant grains because ΔP was <0.25 MPa under all operating conditions. The combustion conditions of the propellant grains are in good consistency with those in the solid rocket motor, and all of the CCPs generated by the propellants could be collected in this way; hence, the CCPs collected in these experiments are available for analysis.

3.3. Characterization Method

A laser diffraction particle size analyzer (Mastersizer 2000, Spectris, Shanghai, China) was used to obtain the particle size distribution of CCPs. The morphology and element distribution of CCPs were investigated using a scanning electron microscope (SEM) (Quanta 650 FEG, FEI, Hillsboro, America) and an energy dispersive spectrometer (EDS) (7021-H, Horiba, Kyoto, Japan). An X-ray diffractometer (XRD) (Empyrean, Spectris, Shanghai, China) was used to obtain the phase composition of the CCPs, while quantitative chemical composition analysis was performed by EDTA complexometric titration, a high-frequency infrared carbon-sulfur analyzer (C996, JIEBO, Jiangsu, China), and an oxygen-nitrogen-hydrogen analyzer (Oxygen-Nitrogen-Hydrogen-3000, NCS, Beijing, China). The specific test scheme used is shown in Figure 4.

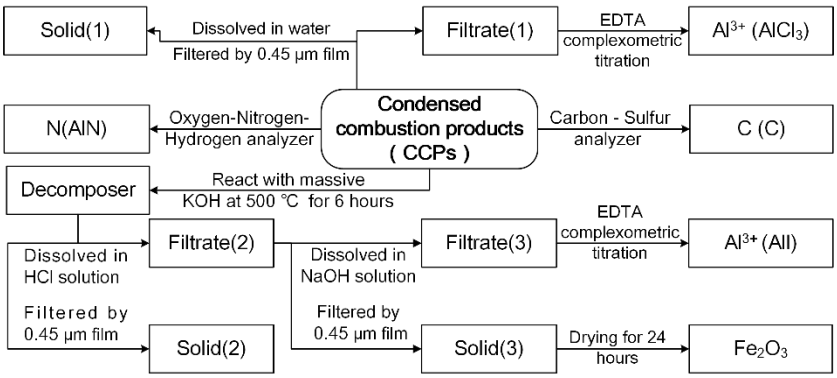

Figure 4. Chemical analysis scheme for CCPs.

During the propellant combustion process, Al particles may be oxidized to Al_2O_3, $AlCl_3$ and AlN, due to the presence of the elements N, Cl, and O. In addition, Fe in catocene may be present in the form of Fe_2O_3 under the operating conditions, and some unburned Al and C may be present in the CCPs. The elemental C content can be measured using a carbon-sulfur analyzer, while the content of O in Al_2O_3 and Fe_2O_3, as well as the content of N in AlN, can be measured using an oxygen-nitrogen-hydrogen analyzer. Furthermore, the concentration of Al^{3+} in solution can be obtained through complexometric titration, while the content of Fe^{3+} can be obtained by alkalization and weighing. For this purpose, a

solution of Fe^{3+} and Al^{3+} may be obtained through alkali fusion of Al_2O_3, $AlCl_3$, AlN, Al, and Fe_2O_3 in the CCPs.

4. Characterization of CCPs

4.1. Morphology and Particle Size of CCPs

It is generally accepted that CCPs consist of aluminum agglomerations and smoke oxide particles. CCPs of the different propellants (named 1#, 2#, 3# and 4#) generated at an initial pressure of 6 MPa were characterized using SEM to compare their particle sizes and morphologies. A series of typical SEM images with different magnifications are shown in Figure 5.

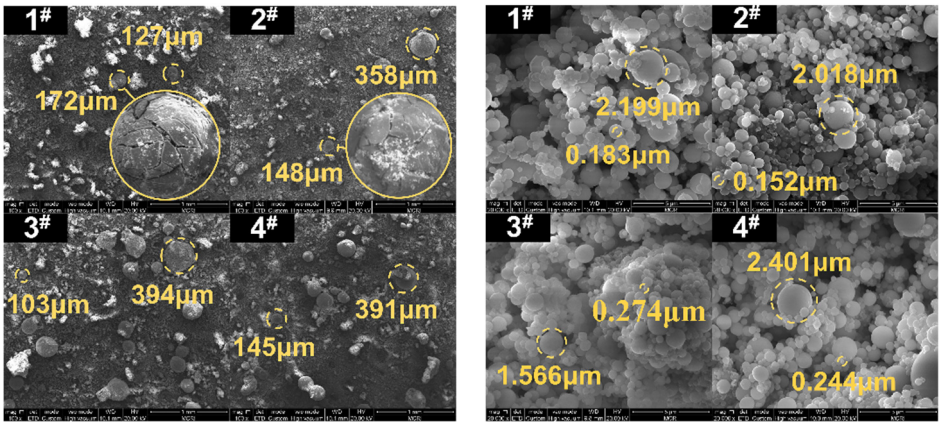

(**a**) (**b**)

Figure 5. SEM images of CCPs at magnifications of (**a**) 100× and (**b**) 20,000×.

The spherical particles in the range of 100–400 μm shown in Figure 5a correspond to aluminum agglomerations, and the partial enlargement of aluminum agglomerations showed that there were many cracks on their surface, which could be explained by the ignition nature of aluminum droplets proposed by Kanian [36]. Aluminum droplets are gradually covered by a thin protective alumina coating during the heating-up stage in the oxidizing atmosphere, and the oxide coating subsequently breaks down as the temperature continues to increase, due to the difference in expansion coefficients between aluminum and alumina coating.

The 0.4–2.5 μm spherical particles with smooth surfaces shown in Figure 5b correspond to smoke oxide particles, and they are presumed to be formed by the burning of aluminum vapor [37]. In addition, numerous smoke oxide clusters are present in CCPs, which are formed by the aggregation of dispersed oxide particles. Therefore, it was necessary to disperse CCPs via ultrasonication, to reveal their real size distribution. Taking into consideration the randomness of sampling, each group of collected CCPs was sampled and tested four times. The particle size distribution and the relative error are shown in Figure 6.

It can be seen from Figure 7 that relative errors were all less than 4.5%, indicating that the collected CCPs were distributed evenly. Particle size distributions for CCPs were bimodal, with a large peak in the range of 0.3–10 μm and a small peak from 15 to 100 μm Only 9.79%, 8.45%, 9.94%, and 3.67% of CCPs had a diameter of over 10 μm for the four propellants. The average particle size of all the samples was <6 μm, which is smaller than the size of virgin aluminum, indicating that The combustion of Al was relatively sufficient at 6 MPa of combustion chamber pressure, and there was no severe agglomeration of Al particles during the process of propellant combustion.

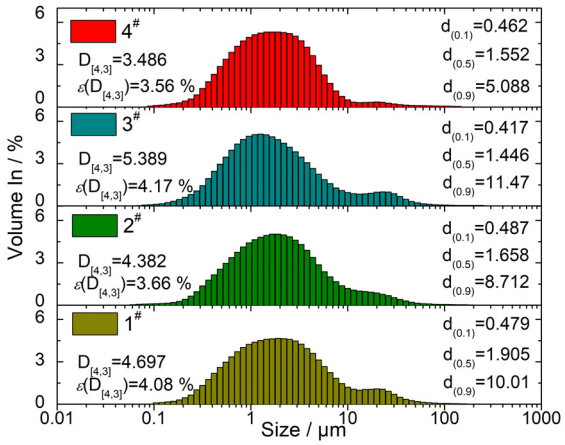

Figure 6. Particle size distributions of CCPs.

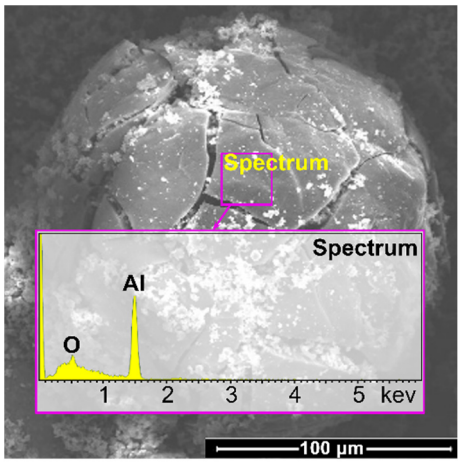

Figure 7. EDS chemical map of CCPs for propellant 2#.

4.2. Chemical Composition of CCPs

The elemental composition of CCPs at an initial pressure of 6 MPa was analyzed using SEM/EDS, and the SEM image and spectra information for CCPs of propellant 2# are shown in Figure 7, while the corresponding elemental data for all the propellants are shown in Table 3.

Table 3. Elemental composition of CCPs.

Propellant No.	Weight Ratio (%)		Atom Ratio (%)	
	Al K	O K	Al K	O K
1#	56.93	43.07	43.92	56.08
2#	53.09	46.91	40.14	59.86
3#	52.16	47.84	39.25	60.75
4#	50.84	49.16	37.99	62.01

The results of the elemental composition indicated that the aluminum agglomeration surface was mainly composed of Al and O, with atomic ratios in accordance with the theoretical value of 2:3, implying that the Al agglomeration was indeed covered by a protective alumina coating, as mentioned in Section 4.1. In addition, XRD was used to determine the phase composition of CCPs, to overcome the limitation of EDS in only being able to measure surface elements, and the results are shown in Figure 8.

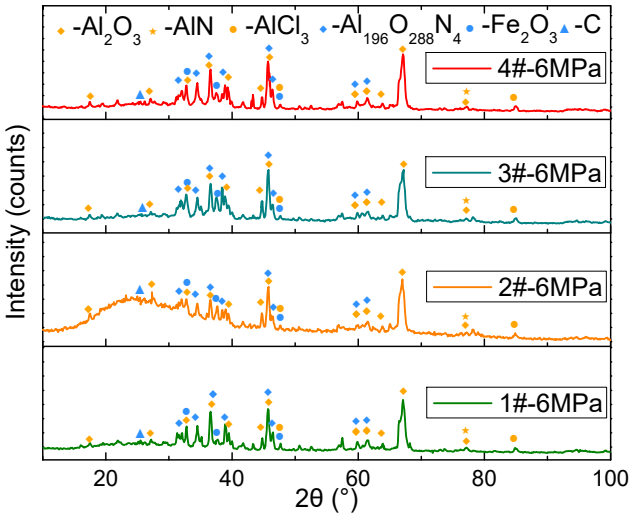

Figure 8. XRD Patterns of CCPs.

Figure 8 shows that the condensed products have the same peak position under different formulations of the propellant at the same pressure, indicating that the components of collected condensed products are basically the same, and mainly consist of C, Al_2O_3, AlN, $AlCl_3$, $Al_{196}O_{288}N_4$, and Fe_2O_3. Moreover, $Al_{196}O_{288}N_4$ can be written in the form $(Al_2O_3)_{96}(AlN)_4$, implying a mixture of Al_2O_3 and AlN. It is worth noting that elemental Al was not detected in the CCPs, because the surface of particles was coated with alumina and Al was inside, and the depth of XRD detection was limited. The C was generated by the incomplete combustion of HTPB. Fe_2O_3 was also found to be present in CCPs, produced by propellant 4# without catocene, which is likely due to small amounts of iron in the inner wall of the steel-collection device being oxidized under the corrosive gas flow. In addition, quantitative analysis of C, Al_2O_3, AlN, $AlCl_3$, Al_2O_3, AlN and Fe_2O_3 was carried out, and the results are shown in Table 4. Taking into consideration the subjectivity of the judgment of indicator discoloration during titration and the randomness of sampling, each group of collected CCPs was sampled and tested four times.

Table 4. Chemical Analysis of CCPs.

Propellant No	Mass Fraction (%)						η_{Al} (%)	ε (η_{Al}) (%)
	C	AlN	Fe_2O_3	Al	Al_2O_3	$AlCl_3$		
1#	0.94	0.79	6.41	2.15	80.63	9.08	95.27	3.62
2#	1.49	3.86	5.47	2.43	84.18	2.57	95.10	4.23
3#	1.52	3.83	6.70	1.06	86.86	0.03	97.86	3.27
4#	0.72	2.05	3.84	0.64	86.43	6.32	98.65	4.36

The combustion efficiency of aluminum η_{Al} may be expressed as:

$$\eta_{Al} = 100 \times \left(1 - \frac{\text{the mass fraction of pure Al}}{\text{total mass fraction of Al}}\right) \quad (3)$$

Table 4 shows that relative errors were all less than 4.5%, indicating that the measurement has high accuracy. CCPs contained high amounts of Al_2O_3, which indicates high reactivity between O and Al during the combustion process. The high values of Al (95–99%) and low elemental Al content (1–2%) indicates that most of the Al particles reacted at an initial pressure of 6 MPa. In addition, there was a small amount of elemental C produced by the incomplete combustion of the binder in CCPs.

4.3. Effect of Pressure

The particle size distributions of CCPs and η_{Al} values generated by propellant 1# at initial pressures of 4 MPa and 6 MPa are shown in Figure 9 and Table 5, respectively.

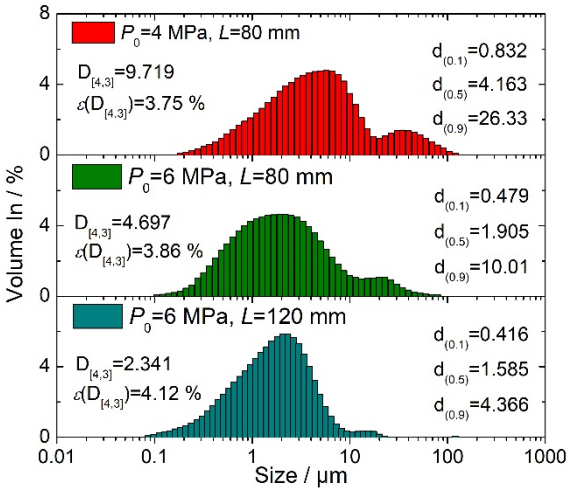

Figure 9. Particle Size Distributions of CCPs.

Table 5. Combustion Efficiencies of Al.

P_0 (MPa)	$\overline{P}$ (MPa)	L (mm)	$\bar{r}$ (mm·s^{-1})	η_{Al} (%)	$\varepsilon(\eta_{Al})$ (%)
4	4.54	80	11.79	93.54	3.48
6	6.57	80	15.06	95.27	4.16
6	6.66	120	14.88	99.01	3.87

A higher initial combustion pressure can reduce the heating time of Al particles on the burning surface, through increasing the burning rate of the propellant, which makes it harder for Al droplets to aggregate. In addition, SEM images of CCPs generated at different initial pressures (Figure 10) shows that the droplets had more cracks on the surface (and hence were more likely to be broken apart) under the large aerodynamic forces caused by high propellant burning rates. Therefore, the average particle size, $D_{[4,3]}$, decreased by 42.97% when the initial pressure increased by 2 MPa.

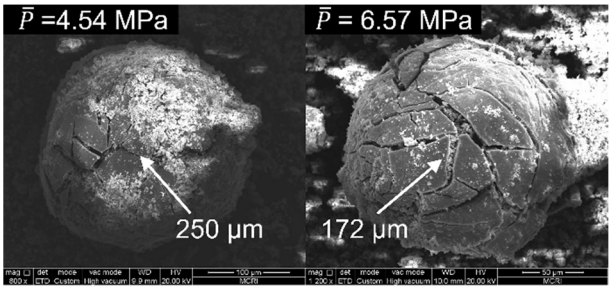

Figure 10. SEM images of agglomerations.

Although both the decrease in particle size and the increased surface-cracking under higher pressures are beneficial to the combustion of Al; its η_{Al} value increased only by 1.73% (from 93.54% to 95.27%), because the high flow velocities generated by a higher burning rate shortened the residence time of Al in the combustion chamber. However, as the residence time depends not only on the flow velocity but also the length of the combustion chamber, increasing the length from 80 mm to 120 mm resulted in an η_{Al} value of 99.01%.

4.4. Effect of Formulation

The particle size distributions of CCPs and η_{Al} values at an initial pressure of 4 MPa are shown in Figure 11 and Table 6, respectively.

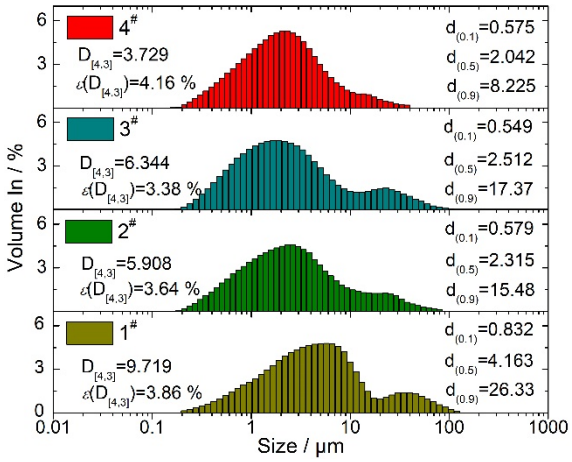

Figure 11. Particle Size Distributions of CCPs.

Table 6. Burning Rates of Propellants and Corresponding Combustion Efficiencies of Al.

Propellant No.	$\bar{r}$ (mm·s^{-1})	η_{Al} (%)	ε (η_{Al}) (%)
1#	11.79	93.54	4.02
2#	12.56	93.93	3.25
3#	13.66	97.00	3.56
4#	8.39	97.49	4.27

Figure 11 showed that the particle size distributions for CCPs of the four propellants were bimodal, which was the same as the results obtained at 6 MPa. The D[3,4] of CCPs was significantly negatively correlated with both the content of fine AP and the content of catocene, while replacing coarse Al with fine Al resulted in an increase in D[3,4] of 0.436 μm in CCPs.

The diffusion combustion between fine AP and HTPB occurring over a smaller scale and the diffusion flame being closer to the burning surface resulted in that Al particles in propellant 2# were more likely to be ignited rather than to agglomerate. Moreover, the addition of fine AP reduces the number density of Al particles in the "pocket" [38], i.e., the gap surrounded by adjacent coarse AP. Therefore, the CCPs of propellant 1# without thin AP had a larger particle size. However, the higher burning rate caused by the smaller diffusion combustion scale was not conductive to the burning out of Al particles, so that the η_{Al} value of propellant 2# only increased by 0.49%, compared to propellant 1#.

The number density decreases with the increase of aluminum particle sizes with the same mass content, in terms of the microstructure, thus the initial aluminum size has a direct bearing on CCPs sizes. As shown in Figure 11, the average diameter of CCPs decreased 0.436 μm when the initial diameter of aluminum particles increased from 13 μm to 23 μm, which was similar to the results obtained by Sambamurthi, using AP/PBAN/Al propellants [29]. The mechanism of Al agglomeration on different initial particle size is shown in Figure 12; 23 μm Al powders tended to ignite individually at the burning surface, because the large distance from each other gave them little opportunity to concentrate before ignition, but the distance between the 13 μm Al powders provided more appropriate conditions for aluminum agglomeration on the burning surface, thus forming relatively large agglomerates. However, Al particles with a large size were more difficult to heat up, and were therefore less likely to be burned out, and thus the η_{Al} value was reduced by 3.07% for propellant 2# with larger virgin aluminum, compared to propellant 3#.

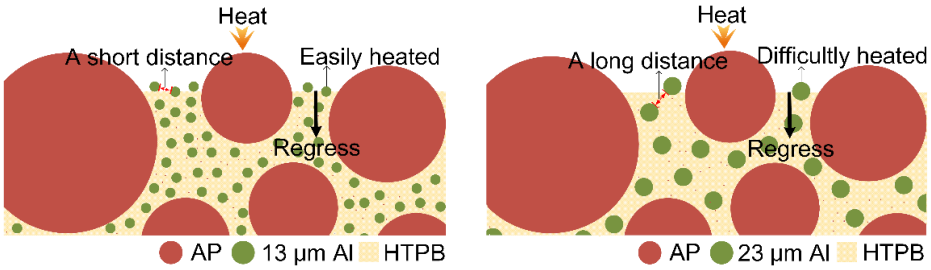

Figure 12. Diagram for the agglomeration mechanisms of (**a**) 13 μm Al and (**b**) 23 μm Al.

The propellant burning rate was increased by reducing the scale of diffusion combustion using catocene. The accelerated decomposition-rate of the binder simultaneously facilitates Al particle agglomeration, although the large aerodynamic forces caused by a high burning-rate facilitates Al particles leaving the burning surface. Therefore, CCPs produced by propellant 4# without catocene featured decreases in Al agglomeration as well as smoke oxide particles, the combined effect of which decreased the particle size of CCPs and slightly increased the η_{Al} value, compared to propellant 3#.

5. Conclusions

(1) A device was designed to collect CCPs in the combustion chamber of a solid rocket motor for propellants with different formulations at different pressures. The experimental results showed that the fluctuation of the working pressure can be controlled to within 0.3 MPa.

(2) CCPs could be distributed into two moods in the intervals 0.3~10 μm and 15~100 μm, and particles <2 μm in size possessed smooth surfaces. Al_2O_3, AlN, $AlCl_3$, $Al_{196}O_{288}N_4$ and Fe_2O_3 were the main components, and the content of Al_2O_3 was the highest.

(3) A noticeable decrease in the average particle size of CCPs was observed under a higher chamber pressure because aluminum was more difficult to agglomerate, but a weak positive correlation was observed between the operating pressure and combustion efficiency of aluminum, due to the short residence time of Al particles in the combustion chamber.

(4) Both the average particle size of CCPs and combustion efficiency of aluminum have a significant negative correlation with the size of virgin aluminum. The increase of fine AP content reduced the agglomeration of aluminum significantly, but had little effect on the combustion efficiency of aluminum. The addition of catocene can increase the content of both the smoke particles and the aluminum agglomerations in CCPs.

The direction of future work should be focused on studying the effects of bimodal size distribution Al, nano Al and the addition of carbon-based functionalized nanostructures.

Author Contributions: Conceptualization, X.-L.L. and L.-L.L.; methodology, X.-L.L., S.-Q.H. and L.-L.L.; software, X.-L.L.; validation, X.-L.L. and L.-L.L.; formal analysis, X.-L.L. and S.-Q.H.; investigation, X.-L.L., S.-Q.H., L.-L.L. and Y.Z.; resources, X.-L.L., S.-Q.H. and L.-L.L.; data curation, X.-L.L. and L.-L.L.; writing—original draft preparation, X.-L.L.; writing—review and editing, L.-L.L.; visualization, X.-L.L.; supervision, X.-L.L.; project administration, S.-Q.H. and Y.Z.; funding acquisition, S.-Q.H. All authors have read and agreed to the published version of the manuscript.

Funding: This research was funded the National Natural Science Foundation of China, Grant No. 51776175.

Institutional Review Board Statement: Not applicable.

Informed Consent Statement: Not applicable.

Data Availability Statement: Not applicable.

Conflicts of Interest: The authors declare no conflict of interest.

Nomenclature

$D_{[4,3]}$	the weighted average of the particle size to the surface area	[μm]
$d_{(0.1)}$	the corresponding particle size when the sum of volume fraction is 10%.	[μm]
$d_{(0.5)}$	the corresponding particle size when the sum of volume fraction is 50%.	[μm]
$d_{(0.9)}$	the corresponding particle size when the sum of volume fraction is 90%.	[μm]
$\overline{P}$	time-averaged pressure	[MPa]
P	pressure	[MPa]
P_{max}	the maximum pressure during combustion	[MPa]
P_{min}	the minimum pressure during combustion	[MPa]
$\overline{r}$	burning rate	[mm·s^{-1}]
t_A	the start time of propellant combustion	[s]
t_B	the end time of propellant combustion	[s]
Δt	burning time	[s]
η_{Al}	the combustion efficiency of aluminum	[%]
ε	relative error	[%]
Abbreviation		
CCPs	condensed combustion products	
HTPB	hydroxyl-terminated polybutadiene	
AP	ammonium perchlorate	
Al	aluminum	
SEM	scanning electron microscope	
EDS	energy disperse spectroscopy	
XRD	x-ray diffraction	

References

1. Sippel, T.R.; Son, S.F.; Groven, L.J. Aluminum agglomeration reduction in a composite propellant using tailored Al/PTFE particles. *Combust. Flame* **2014**, *161*, 311–321. [CrossRef]
2. Liu, T.K.; Perng, H.C.; Luh, S.P.; Liu, F. Aluminum agglomeration in ammonium perchlorate/cyclotrimethylene trinitramine/aluminum/hydroxy-terminated polybutadiene propellant combustion. *J. Propuls. Power* **1992**, *8*, 1177–1184. [CrossRef]
3. Yuan, J.F.; Liu, J.Z.; Zhou, Y.N.; Wang, J.R.; Xv, T.W. Aluminum agglomeration of AP/HTPB composite propellant. *Acta Astronaut.* **2019**, *156*, 14–22. [CrossRef]
4. Orlandi, O.; Plaud, M.; Godfroy, F.; Larrieu, S.; Cesco, N. Aluminium droplets combustion and SRM instabilities. *Acta Astronaut.* **2019**, *158*, 470–479. [CrossRef]
5. Babuk, V.A.; Vassiliev, V.A.; Sviridov, V.V. Propellant formulation factors and metal agglomeration in combustion of aluminized solid rocket propellant. *Combust. Sci. Technol.* **2001**, *163*, 261–289. [CrossRef]
6. Liu, T.K. Experimental and model study of agglomeration of burning aluminized propellants. *J. Propuls. Power* **2005**, *21*, 797–806. [CrossRef]
7. Mullen, J.C.; Brewster, M.Q. Reduced agglomeration of aluminum in wide-distribution composite propellants. *J. Propuls. Power* **2011**, *27*, 650–661. [CrossRef]
8. Babuk, V.A.; Vasil'Ev, V.A.; Potekhin, A.N. Experimental investigation of agglomeration during combustion of aluminized solid propellants in an acceleration field. *Combust. Explos. Shock Waves* **2009**, *45*, 32–39. [CrossRef]
9. Liu, M.; Liu, Z.; Li, S.; Yu, W.; Cao, J.; Wang, N. Study on size distribution and flow characteristics of condensed products in solid rocket motor. *Int. J. Aerosp. Eng.* **2021**, *5*, 5481436. [CrossRef]
10. DeLuca, L.T.; Maggi, F.; Dossi, S.; Weiser, V.; Franzin, A.; Gettwert, V.; Heintz, T. High-energy metal fuels for rocket propulsion: Characterization and performance. *Chin. J. Explos. Propellants* **2013**, *6*, 1–14. [CrossRef]
11. Glotov, O.G. Condensed combustion products of aluminized propellants. III. Effect of an inert gaseous combustion environment. *Combust. Explos. Shock Waves* **2002**, *38*, 92–100. [CrossRef]
12. Takahashi, K.; Oide, S.; Kuwahara, T. Agglomeration characteristics of aluminum particles in AP/AN composite propellants. *Propellants Explos. Pyrotech.* **2013**, *38*, 555–562. [CrossRef]
13. Fukuchi, A.B. Effect of aluminum particle size on agglomeration size and burning rate of composite propellant. *J. Therm. Sci. Technol.* **2022**, *17*, 321–346. [CrossRef]
14. DeLuca, L.T.; Galfetti, L.; Maggi, F.; Colombo, G.; Bandera, A.; Cerri, S.; Donegà, P. Burning of metallized composite solid rocket propellants: Toward nanometric fuel size. In Proceedings of the 2nd International Symposium on Propulsion for Space Transportation, Heraklion, Greece, 5–8 May 2008.

15. Bhadran, A.; Manathara, J.G.; Ramakrishna, P.A. Thrust Control of Lab-Scale Hybrid Rocket Motor with Wax-Aluminum Fuel and Air as Oxidizer. *Aerospace* **2022**, *9*, 474. [CrossRef]
16. Paravan, C. Nano-Sized and Mechanically Activated Composites: Perspectives for Enhanced Mass Burning Rate in Aluminized Solid Fuels for Hybrid Rocket Propulsion. *Aerospace* **2019**, *6*, 127. [CrossRef]
17. Sippel, T.R.; Son, S.F.; Groven, L.J.; Zhang, S.; Dreizin, E. Exploring mechanisms for agglomerate reduction in composite solid propellants with polyethylene inclusion modified aluminum. *Combust. Flame* **2015**, *162*, 846–854. [CrossRef]
18. Lade, R.; Wasewar, K.; Sangtyani, R.; Kumar, A.; Shende, D.; Peshwe, D. Influence of the addition of aluminium nanoparticles on thermo-rheological properties of hydroxyl-terminated polybutadiene-based composite propellant and empirical modelling. *J. Therm. Anal. Calorim.* **2019**, *138*, 211–223. [CrossRef]
19. Liu, X.; Ao, W.; Liu, H.; Liu, P. Aluminum Agglomeration on Burning Surface of NEPE Propellants at 3–5 MPa. *Propellants Explos. Pyrotech.* **2017**, *42*, 260–268. [CrossRef]
20. Tejasvi, K.; Venkateshwara, R.V.; PydiSetty, Y.; Jayaraman, K. Studies on Aluminum Agglomeration and Combustion in Catalyzed Composite Propellants. *Combust. Explos. Shock Waves* **2021**, *57*, 203–214. [CrossRef]
21. Jayaraman, K.; Chakravarthy, S.R.; Sarathi, R. Quench collection of nano-aluminium agglomerates from combustion of sandwiches and propellants. *Proc. Combust. Inst.* **2011**, *33*, 1941–1947. [CrossRef]
22. Zhang, M.; Zhao, F.; Wang, Y.; Chen, X.; Pei, Q.; Xu, H.; Hao, H.; Yang, Y.; Li, H. Evaluation of graphene-ferrocene nanocomposite as multifunctional combustion catalyst in AP-HTPB propellant. *Fuel* **2021**, *302*, 121229. [CrossRef]
23. Jeenu, R.; Pinumalla, K.; Deepak, D. Size Distribution of Particles in Combustion Products of Aluminized Composite Propellant. *J. Propuls. Power* **2010**, *26*, 715–723. [CrossRef]
24. Jin, B.-N.; Wang, Z.-X.; Xu, G.; Ao, W.; Liu, P.-J. Three-dimensional spatial distributions of agglomerated particles on and near the burning surface of aluminized solid propellant using morphological digital in-line holography. *Aerosp. Sci. Technol.* **2020**, *106*, 106066. [CrossRef]
25. Ao, W.; Liu, X.; Rezaiguia, H.; Liu, H.; Wang, Z.; Liu, P.J. Aluminum agglomeration involving the second mergence of agglomerates on the solid propellants burning surface: Experiments and modeling. *Acta Astronaut.* **2017**, *136*, 219–229. [CrossRef]
26. Babuk, V.A.; Vasilyev, V.A.; Malakhov, M.S. Condensed Combustion Products at the Burning Surface of Aluminized Solid Propellant. *J. Propuls. Power* **1999**, *15*, 783–793. [CrossRef]
27. Anand, K.V.; Roy, A.; Mulla, I.; Balbudhe, K.; Jayaraman, K.; Chakravarthy, S.R. Experimental data and model predictions of aluminium agglomeration in ammonium perchlorate-based composite propellants including plateau-burning formulations. *Proc. Combust. Inst.* **2013**, *34*, 2139–2146. [CrossRef]
28. Glotov, O.G. Condensed combustion products of aluminized propellants. IV. Effect of the nature of nitramines on aluminum agglomeration and combustion efficiency. *Combust. Explos. Shock Waves* **2006**, *42*, 436–449. [CrossRef]
29. Sambamurthi, J.K.; Price, E.W.; Sigman, R.K. Aluminum Agglomeration in Solid-Propellant Combustion. *AIAA J.* **1984**, *22*, 1132–1138. [CrossRef]
30. Jayaraman, K.; Anand, K.V.; Chakravarthy, S.R.; Sarathi, R. Effect of nano-aluminium in plateau-burning and catalyzed composite solid propellant combustion. *Combust. Flame* **2009**, *156*, 1662–1673. [CrossRef]
31. Jayaraman, K.; Chakravarthy, S.R.; Sarathi, R. Accumulation of nano-aluminium during combustion of composite solid propellant mixtures. *Combust. Explos. Shock Waves* **2010**, *46*, 21–29. [CrossRef]
32. Tejasvi, K.; Venkateshwara Rao, V.; Pydi Setty, Y.; Jayaraman, K. Ultra-Fine Aluminium Characterization and its Agglomeration Features in Solid Propellant Combustion for Various Quenched Distance and Pressure. *Propellants Explos. Pyrotech.* **2020**, *45*, 714–723. [CrossRef]
33. Babuk, V.A.; Dolotkazin, I.N.; Glebov, A.A. Burning Mechanism of Aluminized Solid Rocket Propellants Based on Energetic Binders. *Propellants Explos. Pyrotech.* **2005**, *30*, 281–290. [CrossRef]
34. Yuan, J.; Liu, J.; Zhou, Y.; Zhang, Y.; Cen, K. Thermal decomposition and combustion characteristics of Al/AP/HTPB propellant. *J. Therm. Anal. Calorim.* **2021**, *143*, 3935–3944. [CrossRef]
35. Liu, T.K.; Hsieh, C.F. Analysis of agglomerate size from burning aluminized AP/RDX/HTPB propellants in quench bomb. *J. Propuls. Power* **1996**, *12*, 995–998. [CrossRef]
36. Sarou-Kanian, V.; Rifflet, J.C.; Millot, F.; Matzen, G.; Gökalp, I. Influence of nitrogen in aluminum droplet combustion. *Proc. Combust Inst.* **2005**, *30*, 2063–2070. [CrossRef]
37. Ao, W.; Liu, P.J.; Yang, W. Agglomerates, smoke oxide particles, and carbon inclusions in condensed combustion products of an aluminized GAP-based propellant. *Acta Astronaut.* **2016**, *129*, 147–153. [CrossRef]
38. Maggi, F.; DeLuca, L.T.; Bandera, A. Pocket Model for Aluminum Agglomeration Based on Propellant Microstructure. *AIAA J.* **2015**, *53*, 3395–3403. [CrossRef]